Dual-Spin Spacecraft Stabilization Using Nutation Feedback and Inertia Coupling

John W. Smay* and Loren I. Slafer*
Hughes Aircraft Company, El Segundo, Calif.

Substantial active nutation control of a dual-spin spacecraft is achieved through augmentation of the fundamental dynamic coupling between the payload azimuth pointing control system and the vehicle nutation dynamics. A significant increase in damping effectiveness over simple dynamic coupling is achieved through integration of a simple rotor-mounted nutation sensing accelerometer with the despun payload control system. This technique is shown to overcome limitations inherent in both passive mechanical damping systems and active nutation control through simple dynamic coupling. The system dynamics and the control laws of the composite nutation and pointing control systems are developed. A closed-form expression for the resulting damping strength is derived. Implementation and functional operation of the control system are discussed. Analysis of the characteristics of the interaction provides design tools for optimization of the system dynamics to achieve maximum effectiveness. A design example is presented for illustration, with simulation results that verify the analytical conclusions.

Nomenclature

I_p, I_s = platform and rotor spin moments of inertia, respectively
I_T = total vehicle transverse moments of inertia
I_{13}, I_{23} = platform products of inertia
σ = inertia ratio (I_s/I_T)
r = $(I_{13}^2+I_{23}^2)^{1/2}/I_T I_p$
ρ_1 = $I_{13}/I_T I_p$
ρ_2 = $I_{23}/I_T I_p$
ρ_0 = $(\rho_1^2+\rho_2^2)^{1/2}$
ϕ_3 = $\tan^{-1}\rho_2/\rho_1 = \tan^{-1} I_{23}/I_{13}$
$P(s)$ = plant matrix of vehicle dynamics
$Q(s)$ = open-loop nutation dipole
r_a = $[r_1, r_2, r_3]$ = radius vector from vehicle c.m. to accelerometer
r_0 = $(r_1^2+r_2^2)^{1/2}$ = transverse component of r_a
ϕ_1 = $\tan^{-1} r_2/r_1$ = angle of r_0 in rotor coordinates
ϕ_2 = shaft angle encoder pulse phase
$H(s)$ = payload pointing loop open-loop transmission (excluding nutation dipole)
$H(j\lambda_n)$ = $\beta e^{j\theta}$
$F_1(s)$, $F_2(s)$ = nutation rate feedback filters operating on signal in rotor and platform coordinates, respectively
$L(s)$ = system open-loop transmission matrix
K_1, K_2, K = nutation rate feedback gains
ω_p, ω_s = nominal platform and rotor inertial angular rate about the spin axis
ω_r = $\omega_s - \omega_p$ = relative angular rate
λ_n, Ω_n = open-loop nutation frequencies in platform and rotor coordinates, respectively
Ω_a = $\omega_s + \omega_r - \lambda_n$ = accelerometer scaling frequency
K_n = $K r_0 \rho_0 \Omega_a/\lambda_n$ = normalized transverse rate feedback gain
ω = $[\omega_1, \omega_2, \omega_3]^T$ = perturbation about nominal of platform rate in platform coordinates
ω_{s1}, ω_{s2} = ω_1, ω_2 in rotor coordinates
θ_p, θ_s = platform and rotor inertial phase (small transverse angle approximation)
$\psi = \omega_r t$ = relative spin phase of rotor and platform
θ_n = nutation half-angle magnitude (small angles)
τ_d = active nutation damping time constant
δ = $1 + 2\omega_p/\lambda_n$
τ_n = $2/(r\lambda_n\delta)$ = normalized nutation damping time constant
MOI = moment of inertia
POI = product of inertia
ACS = attitude control system
ACE = attitude control electronics
DBA = despin bearing assembly
SAE = shaft angle encoder

I. Introduction

FOR a dual-spin spacecraft, stabilization of the vehicle attitude (i.e., maintaining the spin axis coaligned with the system angular momentum vector) typically has been achieved with the use of mechanical elements located on the spacecraft which provide the energy dissipation required to remove transverse angular momentum. Transient nutation motion of the vehicle will be induced through motion of any articulated payload elements and through the firing of control thrusters during attitude and orbit correction maneuvers. Residual, steady-state nutation may develop from the effects of flexible elements or sloshing liquids on the spacecraft. The dynamics and stability criteria for a dual-spin spacecraft are well understood,[1-4] and will not be repeated here. The configuration has been demonstrated successfully in many military, scientific, and commerical applications, including TACSATCOM I, DSCS II, INTELSATS III, IV and IVA, the Canadian and Western Union Domestic Communication Satellites, and the Orbiting Solar Observatory series.

For a spacecraft configuration in which the rotor spin inertia exceeds the total vehicle transverse inertia ($\sigma > 1$), the rotor spins about the vehicle axis of maximum moment of inertia (the system minimum energy state and, hence, an inherently stable configuration). Asymptotic stability is achieved with the inclusion of an energy dissipating passive damping mechanism located on either the spinning or despun elements. Here the nutation damping (such as is provided by a mercury filled tube mounted to the spinning rotor) will augment natural stabilizing dissipation from such elements as fuel slosh or structural flexing to improve the nutation transient

Received Feb. 27, 1976; revision received June 1, 1976. The authors would like to acknowledge H. Rosen and J.O. Salvatore who initially conceived the technique utilizing the rotor nutation accelerometer for continuous active nutation control.
Index category: Spacecraft Attitude Dynamics and Control.
*Group Head, Guidance and Control Systems Laboratory, Space and Communications Group. Member AIAA.

settling time and maintain the required payload pointing accuracy.

For a vehicle configuration in which the rotor spins about the spacecraft axis of minimum moment of inertia ($\sigma < 1$), the system highest energy state), asymptotic stability is achieved only if energy dissipation on the despun element exceeds energy dissipation on the spinning rotor. For this configuration energy dissipation on the rotor acts as a destabilizing influence, attempting to force the system to its minimum energy state. An eddy-current pendulum-type damper, mounted to the despun payload frequently is used to perform the necessary nutation damping function. The INTELSAT IV and IVA synchronous orbit communication satellites are examples of such systems. Thus, for this configuration, energy dissipation on the despun payload must both establish the fundamental system stability and also must provide the desired nutation transient settling time.

For a spacecraft configuration in which the despun payload possesses a product of inertia (*POI*) between the spin and transverse axes, it has been shown[5-8] that nutation can be controlled actively onboard through the use of properly generated control torques about the spin axis. Reference 8 presented a closed-form solution to the problem of the interaction of the payload pointing control system and vehicle nutation, deriving an analytical expression for the resulting closed-loop nutation damping time constant.

Use of the payload pointing control system for active nutation control to augment the passive dampers via the *POI* dynamic coupling was shown[8] to have fundamental limitations on the strength of the achievable nutation damping. These limitations are imposed by the combined effects of the required control system stability margins, and the ratio of the *POI* to both the vehicle transverse moment of inertia (*MOI*) and payload *MOI* about the spin axis. As the magnitude of the *POI* is reduced relative to the platform spin and vehicle transverse inertias, the resulting active nutation damping becomes less effective with no compensation achievable through modification of the control system design.

This paper presents a technique which circumvents these problems, describing a system which can provide significant active nutation control using *POI* dynamic coupling. It will be shown that, for a vehicle with a relatively small payload *POI*, greater than an order of magnitude reduction in damping time constant over that obtained from simple dynamic coupling is realizable. In addition, the system will adapt to a wide range of nutation frequencies. For a minimum required *POI*, this technique could provide sufficient active stabilization so as to eliminate the need for passive stabilization devices with a resulting cost and weight savings. The control scheme uses transverse rate feedback as sensed by a rotor-mounted accelerometer to provide an additional feedback path in the control system. The use of a rotor-mounted accelerometer for active onboard control of nutation using the spacecraft thrusters is a well-established technique for attitude stabilization.[9] By utilizing this simple sensing technique, modified to operate in a despun reference frame, an additional input to the control system is available which provides a greater degree of independence in the design of the pointing control and nutation damping functions using the same controller—the despin torque motor. Section II of the paper describes an attitude control system (*ACS*) configuration for which this technique easily could be adapted, outlining the functional operation and implementation of the pointing control system and integration of the active nutation control function into the overall system. Section III of the paper presents the system dynamics and nutation sensing equations. In Sec. IV the control system design analysis is presented, developing a closed-form expression for the resulting nutation damping time constant. Parameter sensitivities are discussed along with effects of the interaction on payload pointing accuracy. Finally, in Sec. V, a design example is presented illustrating application of the technique to one class of spacecraft. Simulation results are presented utilizing a breadboard of the control electronics which verify the analytical conclusions.

II. Control System Implementation and Functional Operation

An example of one class of dual-spin spacecraft configuration to which this nutation control concept could be applied is the INTELSAT IVA communication satellite shown in Fig. 1, the first two of which presently are operating in synchronous orbit. The vehicle utilizes the Hughes' Gyrostat configuration with a vehicle inertia ratio ranging from 0.20 to 0.25. The spacecraft is comprised of a spinning rotor containing the propulsion, power, attitude control, and a portion of the telemetry and command subsystems, and a despun, Earth-oriented communications platform. The platform contains shaped beam and global coverage antennas, the communication subsystem, the remaining portion of the telemetry and command subsystem, and the pendulum-type nutation dampers providing attitude stabilization.

As can be seen in Fig. 1, the design of the despun platform structure is such that a dynamic imbalance will exist, with a product of inertia between the spin and transverse axes of the spacecraft. The mass properties of INTELSAT IVA are such that the magnitude of the *POI* is 13% of the platform spin *MOI* and 1.5% of the transverse *MOI*. For an optimum control system design, the minimum active nutation time constant achievable with these constraints is ~500 sec. Each passive damper provides a 60-sec damping time constant at its resonance. Thus, mass property limitations would not allow sufficient active control to provide damping equivalent to that of a mechanical damper.

The basic control system configuration which can provide both continuous pointing control of the despun payload about the vehicle spin axis and active nutation damping is illustrated in the functional block diagram of Fig. 2. The design is based on the concept of integrating all control system elements (sensors and actuators) within the spinning portion of the spacecraft.

In operation, the inertial boresight of the despun payload is derived through phase and frequency comparison of the once-

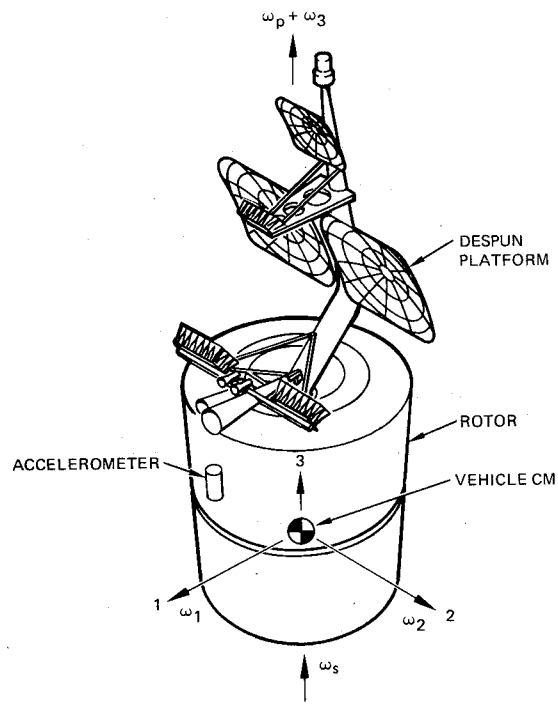

Fig. 1 INTELSAT IVA dual-spin spacecraft and coordinate definition.

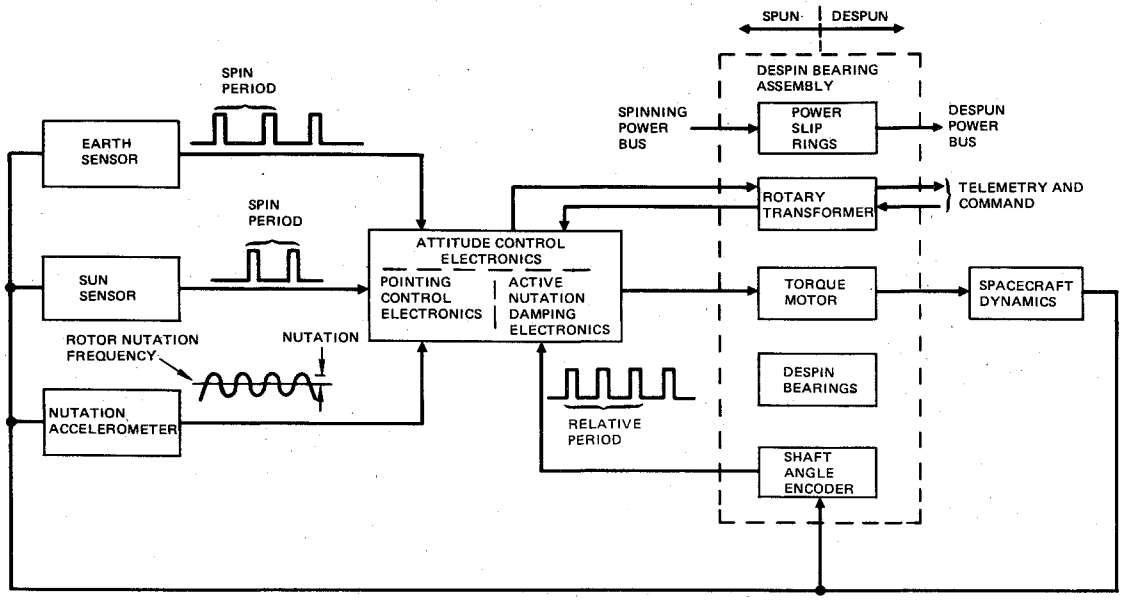

Fig. 2 Pointing and nutation control system functional block diagram.

per-spin-cycle pulse outputs of the inertial attitude sensors (sun or Earth) with the output of a shaft angle encoder (*SAE*, optical or magnetic) contained within the design bearing assembly (*DBA*). The encoder output supplies information relating the phase and rate of the despun payload to the spinning rotor. The sensor outputs are processed by the attitude control electronics (*ACE*) which perform pointing error detection and provide generation of the feedback control signals to the *ACS* control element, an electric torque motor contained in the bearing assembly (the spinning/despun interface). For a Gyrostat vehicle configuration (as is INTELSAT IVA) a rotor-mounted nutation sensing accelerometer is utilized in conjunction with the axial thrusters for active nutation control for failure mode attitude stabilization. Thus, the existing accelerometer is available (on the rotor) for use in the active nutation damping function without requiring an additional nutation sensor.

The rotor nutation accelerometer, *SAE*, and motor-control elements of the pointing system comprise the active nutation damping function. The accelerometer signal processing and nutation control torque generation are implemented within the *ACE*. Functionally, the nutation accelerometer output signal is prefiltered (to remove high-frequency noise and any dc offset), generating, as will be discussed in Sec. III, a signal at rotor nutation frequency. The filtered output is modulated by a reference square-wave signal created from the *SAE* output pulse train. The *SAE* frequency represents the rotor-to-payload relative frequency, and, thus, the modulation process performs the required coordinant transformation generating a signal at platform nutation frequency. The modulator output then is filtered to remove its high-frequency harmonics and dc components. The remaining fundamental frequency then is scaled to provide a sinusoidal motor torque command whose amplitude is proportional to the nutation angle. The nutation torque command is summed with the pointing feedback control torque command to drive the despin motor. To optimize the damping effectiveness, the desired total phase angle of the feedback (discussed in Sec. III) is set by mechanical alignment of the encoder phasing with respect to the accelerometer. Based on inflight studies of the INTELSATs IV and IVA nutation accelerometer performance, it is expected that the system will operate smoothly to nutation angles well below 0.005°.

The following two sections present the analysis of the nutation control system, discussing the sensing and control dynamics, and deriving design equations for application of the nutation control technique.

III. Vehicle Equations of Motion

Vehicle Dynamics

A representative sketch of the dual-spin spacecraft under investigation is depicted in Fig. 1. The spinning rotor with appropriate nutation damping provides basic attitude stability through gyroscopic stiffness, while a nominally despun platform supports a payload. A platform fixed coordinate system is defined with origin at the vehicle c.m. and 3 axis along the vehicle spin axis. Symmetric transverse inertias and a balanced rotor are assumed here to simplify the discussion. Body rates in platform coordinates are expressed as $[\omega_1, \omega_2, \omega_3+\omega_p]^T$, where $\omega=[\omega_1, \omega_2, \omega_3]^T$ represents small rate perturbations about the nominal $[0, 0, \omega_p]^T$. The case of most interest is with the platform despin ($\omega_p=0$); however, this generality is retained as it is frequently desirable to spin the platform slowly for short periods during a mission. Then the vehicle small angle torque equations linearized about the nominal rate and expressed in the platform coordinate frame may be written

$$\dot{\omega}_1+\lambda_n\omega_2=(I_{13}/I_T)\dot{\omega}_3 - (I_{23}/I_T)(\omega_p^2+2\omega_p\omega_3)+E_1/I_T \tag{1a}$$

$$\dot{\omega}_2-\lambda_n\omega_1=(I_{23}/I_T)\dot{\omega}_3 + (I_{13}/I_T)(\omega_p^2+2\omega_p\omega_3)+E_2/I_T \tag{1b}$$

$$\dot{\omega}_3=(I_{13}/I_p)\dot{\omega}_1+(I_{23}/I_p)\dot{\omega}_2+(I_{23}/I_p)\omega_p\omega_1 - (I_{13}/I_p)\omega_p\omega_2+T_3/I_p+E_3/I_p \tag{1c}$$

$$\dot{\omega}_s=-T_3/I_s+E_s/I_s \tag{1d}$$

where T_3 is the internal 3-axis torque, the E's are external torques, and

$$\lambda_n=[(I_p-I_T)\omega_p+I_s\omega_s]/I_T \tag{2}$$

is the platform nutation frequency. Transforming, collecting terms in ω, and inverting, one obtains the rate vector in terms of input torques T, and the plant matrix as

$$\omega = PT \tag{3}$$

where

$$P = \frac{1}{\Delta}\begin{bmatrix} [s^2(1-\rho_2 I_{23}) - s\omega_p \rho_1 I_{23} + 2\omega_p^2 \rho_1 I_{13}]/I_T \\ [s^2 \rho_2 I_{13} + s\{\lambda_n + \omega_p(\rho_2 I_{23} + 2\rho_1 I_{13})\} + 2\omega_p^2 \rho_1 I_{23}]/I_T \\ [s^2 \rho_1 + s\rho_2(\omega_p + \lambda_n) - \omega_p \lambda_n \rho_1] \end{bmatrix}$$

$$\begin{bmatrix} [s^2 \rho_1 I_{23} - s\{\lambda_n + \omega_p(\rho_1 I_{13} + 2\rho_2 I_{23})\} + 2\omega_p^2 \rho_2 I_{13}]/I_T \\ [s^2(1-\rho_1 I_{13}) + s\omega_p \rho_2 I_{13} + 2\omega_p^2 \rho_2 I_{23}]/I_T \\ [s^2 \rho_2 - s\rho_1(\omega_p + \lambda_n) - \omega_p \lambda_n \rho_2] \end{bmatrix}$$

$$\begin{bmatrix} [s^2 \rho_1 - s(\lambda_n \rho_2 + 2\omega_p \rho_1) + 2\lambda_n \omega_p \rho_1 \\ [s^2 \rho_2 + s(\lambda_n \rho_1 + 2\omega_p \rho_2) - 2\lambda_n \omega_p \rho_2] \\ [s^2 + \lambda_n^2]/I_p \end{bmatrix} \tag{4a}$$

with

$$\Delta(s) = s[(1-r)s^2 + (\lambda_n^2 + r\omega_p(3\lambda_n + 2\omega_p))] \tag{4b}$$

$$r = [I_{13}^2 + I_{23}^2]/I_T I_p \tag{4c}$$

$$\rho_1 = I_{13}/I_T I_p, \quad \rho_2 = I_{23}/I_T I_p \tag{4d}$$

The elements from the third column of P and pertinent torque feedback paths are diagrammed as Fig. 3. Let $T = T_b + T_e$, with

$$T_b = -G\omega = -\begin{bmatrix} 0 & 0 & 0 \\ 0 & 0 & 0 \\ K_1 & K_2 & I_p s H(s) \end{bmatrix} \omega \tag{5}$$

as feedback torques and T_e representing all remaining torques. K_1, K_2 couple the transverse rates back to the despin motor and $I_p s H(s)$ feeds back platform position. For later convenience, this term is expressed such that $H(s)$ is the entire 3-axis loop transmission, excluding only the nutation dipole Q in evidence in Eq. (4). Substituting in Eq. (3), this expression is rearranged to

$$\omega = [I+PG]^{-1} PT_e = [I+L]^{-1} PT_e \tag{6}$$

Stability of the closed-loop system is predicted by the zeros of the determinant of the return difference matrix $I+L$. Denoting this determinant as $\Delta_c(s)$, and substituting elements of P from Eq. (4)

$$\begin{aligned} \Delta_c(s) &= I + P_{13}K_1 + P_{23}K_2 + P_{33} I_p s\, H(s) \\ &= \{s[s^2 + \lambda_n^2] H(s) + [I-r]s^3 + [\rho_1 K_1 + \rho_2 K_2]s^2 \\ &\quad + [\lambda_n^2 + (\lambda_n + 2\omega_p)(\rho_1 K_2 - \rho_2 K_1) + r\omega_p(3\lambda_n + 2\omega_p)]s \\ &\quad - 2\omega_p \lambda_n [\rho_1 K_1 + \rho_2 K_2]\}/\Delta(s) \end{aligned} \tag{7}$$

Given rational functions for the feedback compensations K_1, K_2, and H, it would be a straightforward task to factor the numerator of Eq. (7) and obtain the closed-loop pole locations. We next turn our attention to obtaining a limited model of the transverse rate feedback gains for a unique hardware mechanization.

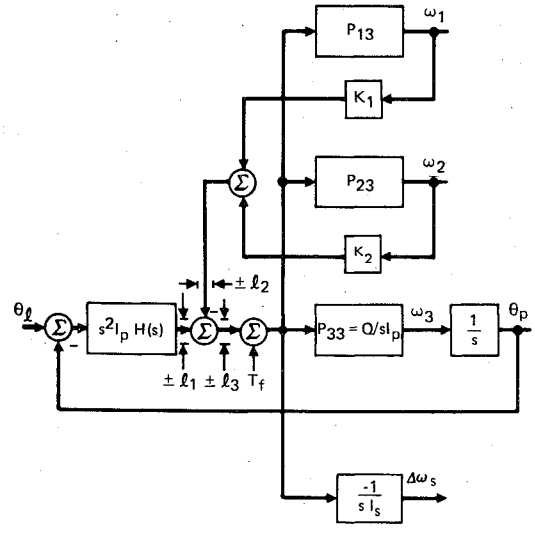

Fig. 3 System diagram of three-axis vehicle dynamics with internal 3-axis torque only.

Nutation Sensing

Some type of angular rate sensor is needed to complete the transverse rate feedback loops shown in Fig. 3. A particularly attractive sensing method described here uses the output of a spinning rotor-mounted accelerometer. The rotor-mounted accelerometer is excited at rotor nutation frequency Ω_n, whereas a feedback torque at platform nutation frequency is needed to damp nutation via the platform product of inertia. A simple frequency shift technique as well as the feedback gain and phase are derived in the following. The transverse rate sensing and processing path is depicted in Fig. 4. A linear accelerometer mounted with sensitive axis parallel to the 3-axis of Fig. 1 at radius $r_a = [r_1, r_2, r_3]^T$ senses acceleration

$$a(t) = [r_2 \dot{\omega}_{s1} - r_1 \dot{\omega}_{s2}] + [r_1 \omega_{s1} + r_2 \omega_{s2}]\omega_s - r_3[\omega_{s1}^2 + \omega_{s2}^2] \tag{8}$$

where ω_{s1}, ω_{s2} are the body transverse rates in rotor coordinates. The free undamped solution of the vehicle torque equations is, in platform coordinates,

$$\begin{bmatrix} \omega_1(t) \\ \omega_2(t) \end{bmatrix} = \omega_0 \begin{bmatrix} \cos(\lambda_n t - \phi_0) \\ \sin(\lambda_n t - \phi_0) \end{bmatrix} \tag{9}$$

Transforming to rotor coordinates

$$\begin{bmatrix} \omega_{s1}(t) \\ \omega_{s2}(t) \end{bmatrix} = \omega_0 \begin{bmatrix} \cos\Psi & \sin\Psi \\ -\sin\Psi & \cos\Psi \end{bmatrix}$$

$$\begin{bmatrix} \cos(\lambda_{nt} - \phi_0) \\ \sin(\lambda_{nt} - \phi_0) \end{bmatrix} = \omega_0 \begin{bmatrix} \cos(\Omega_n t - \phi_0) \\ \sin(\Omega_n t - \phi_0) \end{bmatrix} \tag{10}$$

where $\Psi = (\omega_s - \omega_p)t = \omega_r t$ is the relative phase between rotor and platform, and $\Omega_n = \lambda_n - \omega_r$ is the nutation frequency observed in rotor fixed coordinates. Defining $\Omega_a = \omega_s + \omega_r - \lambda_n$, substituting Eq. (10) and its derivative in Eq. (8), and neglecting second-order terms

$$\begin{aligned} a(t) &= \Omega_a[r_1 \omega_{s1}(t) + r_2 \omega_{s2}(t)] \\ &= \Omega_a \omega_0 [r_1 \cos(\Omega_n t - \phi_0) + r_2 \sin(\Omega_n t - \phi_0)] \\ &= r_0 \sigma \omega_s \Omega_a \theta_n \cos(\Omega_n t - \phi_0 - \phi_1) \end{aligned} \tag{11}$$

with the nutation angle written as $\theta_n = \omega_0/\sigma\omega_s$ for small angles, $r_0 = (r_1^2 + r_2^2)^{1/2}$ and $\phi_1 = \tan^{-1} r_2/r_1$. Thus, for constant rotor and platform spin rates and sinusoidal nutation, the accelerometer output is a linear combination of the vehicle transverse rates expressed in rotor coordinates. This is the type of nutation feedback signal desired except that it must be shifted back to the platform coordinate frame to be applied coherently as a despin torque relative to nutation in platform coordinates.

We have seen previously in Eq. (10) that for sinusoidal motion the coordinate translation is simply a frequency shift (modulation). A two pulse per revolution shaft angle encoder between rotor and platform is used to generate an index pulse train from which the modulator reference square wave

$$m(t) = \frac{4}{\pi} \sum_{n=1,3,5,\ldots} \frac{\cos[n(\omega_r t - \phi_2)]}{n} \tag{12}$$

is obtained. Multiplying $a(t)$ by this reference and retaining only the platform nutation frequency harmonic, we have

$$z(t) = \frac{2\Omega_a \omega_0}{\pi} [r_1 \cos(\lambda_n t - \phi_2 - \phi_0) + r_2 \sin(\lambda_n t - \phi_2 - \phi_0)]$$

$$= \frac{2r_0\Omega_a}{\pi} [\cos(\phi_1 + \phi_2)\omega_1(t) + \sin(\phi_1 + \phi_2)\omega_2(t)] \tag{13}$$

The signal then is used to generate a despin torque command

$$T_3(t) = \pi K z(t)/2 = -K_1\omega_1(t) - K_2\omega_2(t) \tag{14}$$

where K is a feedback gain in lb-sec^2, and

$$K_1 = -Kr_0\Omega_a \cos(\phi_1 + \phi_2) \tag{15a}$$

$$K_2 = -Kr_0\Omega_a \sin(\phi_1 + \phi_2) \tag{15b}$$

The filters F_1, F_2 are assumed normalized to unity gain at their applicable nutation frequencies Ω_n, λ_n. At other frequencies they may be designed to remove unwanted signal components, e.g., ac coupling and noise and modulation harmonic rejection.

Finally, the coefficients needed in Eq. (7) are derived. Defining $\rho_0 = (\rho_2^2 + \rho_2^2)^{1/2}$, $\phi_3 = \tan^{-1}\rho_2/\rho_1$, and a normalized feedback gain $K_n = Kr_0\rho_0\Omega_a/\lambda_n$, the resultant coefficients are

$$\rho_1 K_2 + \rho_2 K_2 = -Kr_0\Omega_a\rho_0 \cos(\phi_1 + \phi_2 - \phi_3) = -\lambda_n K_n \cos\phi \tag{16a}$$

$$\rho_1 K_2 - \rho_2 K_1 = -Kr_0\Omega_a\rho_0 \sin(\phi_1 + \phi_2 - \phi_3) = -\lambda_n K_n \sin\phi \tag{16b}$$

where K_n, ϕ are the feedback gain and phase. It can be shown that ϕ is the spatial angle between the nutation transverse rate vector and the net transverse torque at the instant this torque is maximum. The two filter phase shifts must of course be accounted for, yielding ϕ in general as

$$\phi = \phi_1 - \angle F_1(j\Omega_n) + \phi_2 - \angle F_2(j\lambda_n) - \phi_3 \tag{17}$$

Undamped sinusoidal motion has been assumed in deriving the coefficients of Eq. (15) so they are valid only when the nutation time constant is suitably greater than the nutation period. The gains are valid for any frequency including the zero frequency limit, but are not meaningful for general transient responses.

Substituting Eq. (16) in Eq. (9), the closed-loop system characteristic equation is written

$$\Delta(s)\Delta_c(s) = s[s^2 + \lambda_n^2]H(s) + [1 - r]s^3 - \lambda_n[K_n\cos\phi]s^2$$

$$+ \lambda_n^2[1 - (1 + 2\omega_p/\lambda_n)K_n\sin\phi + r(\omega_p/\lambda_n)(3 + 2\omega_p/\lambda_n)]s$$

$$+ \lambda_n^3[2(\omega_p/\lambda_n)K_n\cos\phi] \tag{18}$$

This equation approximates the system poles under sinusoidal nutation motion, and hence yields the desired nutation poles.

IV. Damping Loop Design Equations

Nutation Time Constant Derivation

The root of primary interest here from the system characteristic equation [Eq. (18)] is the closed-loop nutation root produced by the nutation pole in Q. The location of the root establishes a stability margin of the vehicle nutation mode and gives the time rate of decay of nutation motion. Again, it is straightforward to factor the numerator polynomial of this equation, solving the analysis problem. With a synthesis goal in mind, however, it is desirable to express the nutation damping behavior directly in terms of relevant system parameters. Important characteristics of the damping scheme are the damping time constant, the effect on platform azimuth pointing, and the damping system linear range. Expressions describing these characteristics are derived in the following in terms of vehicle constants and feedback loop gains and phases.

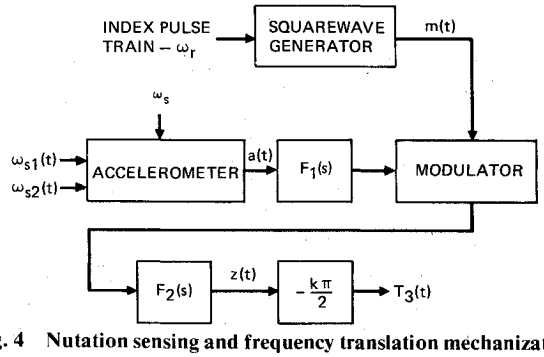

Fig. 4 Nutation sensing and frequency translation mechanization.

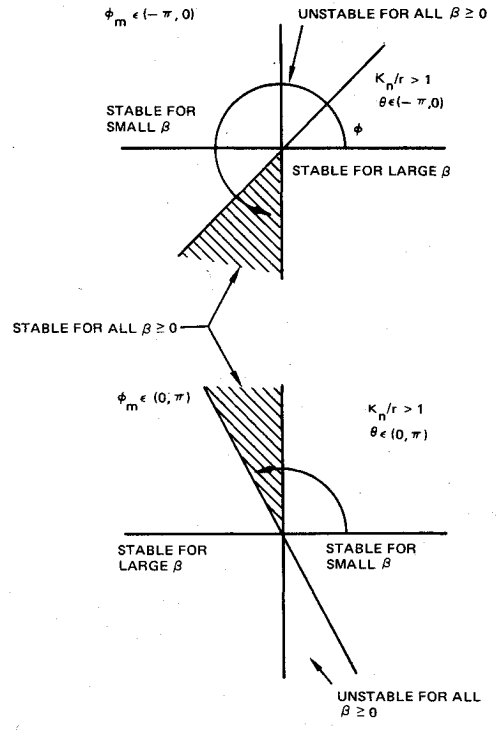

Fig. 5 Nutation root stability variation as a function of ϕ for $K_n/r \approx 1$.

On a root locus plot, the nutation root tends to move from its open-loop position at $\lambda_n/(1-r)^{1/2}$ to the zero of the nutation dipole at λ_n. Setting the restriction that $r<<1$, which is the case in practical satellite design, these two points are very close. This observation, combined with the restriction that the damping time constant be long compared to the nutation period, leads to the conclusion that the closed-loop root $s_1 \cong \lambda_n \cong \lambda_n/(1-r)^{1/2}$, at least for a significant class of vehicles of interest. Thus, we take

$$s_1 = \Delta s + j\lambda_n \tag{19}$$

assuming $|\Delta s| << \lambda_n$. Next, we require that the 3-axis loop transmission $H(s)$ be well-behaved in a neighborhood of s_1 such that the approximation

$$H(s_1) \cong H(j\lambda_n) = \beta e^{j\theta} \tag{20}$$

will hold. β and θ are, respectively, the open-loop gain and phase of the despin loop of Fig. 3 at open-loop nutation frequency when the dipole Q is excluded. Equation (18) now is set equal to zero with Eqs. (19) and (20) substituted, and the resultant expression solved for $Re[\Delta s]$. Dropping second and higher order terms in Δs and r, and making use of $r<<1$, the resultant damping time constant is

$$\tau_d = -1/R_e[\Delta s]$$

$$\cong -\frac{\tau_n\left[1+\beta^2+2\beta\cos\theta+\frac{\delta K_n\sin\phi}{4}\left[4+4\beta\cos\theta+\delta K_n\sin\phi\right]+K_n\cos\phi\left[\beta\sin\theta+K_n\cos\theta\right]\right]}{\left[(1+\omega_p/\lambda_n)\beta\sin\theta+\frac{K_n\beta}{r}\left[\cos\phi\cos\theta-\sin\phi\sin\theta\right]+\frac{K_n}{r}\cos\phi\left[1+\frac{\delta K_n}{2}\sin\phi\right]+(1+\omega_p/\lambda_n)\delta K_n\cos\phi\right]} \tag{21}$$

where $\delta = 1+2\omega_p/\lambda_n$, and $\tau_n = 2/(r\lambda_n\delta)$. This root perturbation technique has been used by previous authors[8,10] to isolate underdamped system roots. The expression remains too complex to provide much design insight so some additional practical simplifications are applied. Observe that $\rho_0 = r/(I_{13}^2+I_{23}^2)^{1/2} < r << 1$; so, in practice, $K_n << 1$ also. Using this we can approximate Eq. (21) in the forms

$$\tau_d \cong \frac{-\tau_n[1+\beta^2+2\beta\cos\theta]}{[(1+\omega_p/\lambda_n)\beta\sin\theta+(K_n\beta/r)\cos(\phi+\theta)+(K_n/r)\cos\phi]}$$

$$= \frac{-\tau_n[1+\beta^2+2\beta\cos\theta]}{(1+\omega_p/\lambda_n)\beta\sin\theta+(K_n/r)(1+\beta^2+2\beta\cos\theta)^{1/2}\cos(\phi+\alpha)} \tag{22}$$

with

$$\alpha = \tan^{-1}[\beta\sin\theta/(1+\beta\cos\theta)] \tag{23}$$

The limiting cases of Eq. (22) now begin to provide the desired design insight.

We note first that the time constant is determined by the composite gain and phase of the two feedback loops of Fig. 3 at the nutation frequency, i.e., β, θ, K_n, and ϕ. Opening the despin loop, the behavior of nutation rate feedback alone is expressed simply as

$$\lim_{\beta\to 0} \tau_d = \frac{-\tau_n}{(K_n/r)\cos\phi} \tag{24}$$

The time constant is inversely proportional to gain and is minimized with ϕ near π. The latter is predicted by our physical interpretation of ϕ at the end of Sec. III. At the other extreme, when the nutation loop is open and the platform is despun ($\omega_p = 0$),

$$\lim_{K_n\to 0} \tau_d = \frac{-\tau_n[1+\beta^2+2\beta\cos\theta]}{\beta\sin\theta} \tag{25}$$

This expression is recognized as the damping time constant attributed to the pointing control system alone, given and analyzed in Ref. 8. It is noted there that the despin loop alone is stabilizing for all β provided $\theta\in(-\pi, 0)$.

Some useful qualitative observations of the nutation time constant behavior follow. First, we note that K_n/r will be the dominant coefficient in the denominator of Eq. (22), giving the time constant closely an inverse proportional dependence on nutation feedback gain K_n. If this coefficient were not dominant, there is little value in having the transverse rate feedback at all. Figure 5 indicates the behavior as a function of $\phi\in(0, 2\pi)$ and $\beta\in(0, \infty)$ with $K_n/r>1$ and θ as a parameter. It is possible to select ϕ, given θ, such that the nutation root is stable for all $\beta\geq 0$ as indicated by the shaded regions. Of course, for sufficiently large β, some other modes of the system will become unstable and stability of the nutation mode is no longer of significance. Shown in Fig. 6 are some parametric plots of τ_d obtained from Eq. (21). Here it is seen that the time constant is minimum with β and θ in the neighborhood of 1 and $-\pi$, respectively. Again the region of nutation mode stability for all $\beta\geq 0$ is shown shaded. For ϕ outside the shaded range, the time constant goes to infinity along an asymptote β_∞, which can be obtained by equating the denominator of Eq. (22) to zero as

$$\beta_\infty = \frac{-(K_n/r)\cos\phi}{\sin\theta+(K_n/r)\cos(\phi+\theta)} \tag{26}$$

for fixed K_n, ϕ, and θ with the platform despun.

The second form in Eq. (22) isolates the nutation rate feedback phase ϕ such that ϕ_m, which minimizes the time constant for fixed despin parameters β, θ, is found as

$$\phi_m = -\alpha-\pi \tag{27}$$

with α given by Eq. (23).

Dependence of τ_d on vehicle spin speed is established by the feedback filters, i.e., $H(s)$ in the despin loop, and F_1, F_2 (including accelerometer scale factor variations) from Fig. 4 in the transverse rate loop. Despin loop parameters tend to a large degree to be set by pointing performance requirements, and, thus, are relatively fixed inputs to the damper design. On the other hand, the transverse rate loop gain and phase are set to achieve desired damping performance. The phase and gain ϕ, K_n can be set independently by appropriately phasing the *SAE*. The result is that filters F_1, F_2 do not have to be sharply tuned to achieve desired performance and the system is only mildly dependent on spin speed. Conversely, mechanical dampers tend to be highly tuned mechanical filters (to maximize damping with minimum weight) which degrade rapidly with vehicle spin speed variations.

Platform Pointing Disturbances Due to Nutation Damping

Since the transverse rate feedback path of Fig. 3 damps nutation by applying a platform despin torque at nutation frequency, this torque must also produce a platform azimuth pointing disturbance of the same frequency. From a func-

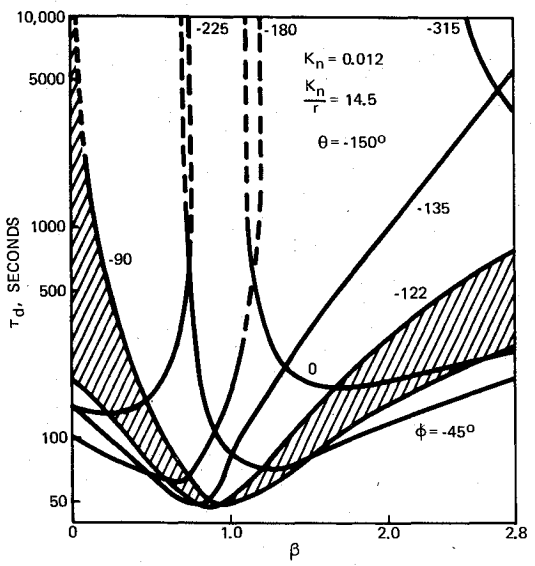

Fig. 6 Nutation time constant vs despin gain. In shaded region nutation root is stable for all $\beta \geq 0$.

tional viewpoint, this pointing disturbance is the primary price paid for the improved nutation damping performance. A useful measure of the disturbance is the ratio of platform pointing angle to nutation angle θ_p/θ_n. Assuming sinusoidal nutation rates of magnitude $\omega_0 = \theta_n \lambda_n$ and using Eqs. (9, 14, and 15), the magnitude of the torque command feedback through the transverse rate loop (see Fig. 3) is $T_n = Kr_0\sigma(2-\sigma)\omega_s^2\theta_n$, with the platform despun. Applying this as a disturbance torque to the platform, the resultant nutation to pointing jitter transmission is

$$\theta_p/\theta_p = Kr_0\sigma(2-\sigma)\omega_s^2 T_D(s) \tag{28}$$

where $T_D(s)$ is the 3-axis torque disturbance transmission function. Noting that pointing disturbances are directly proportional to K whereas the time constant is inversely proportional, we see that a major design tradeoff exists between the speed of nutation damping and permissible pointing disturbances.

Large Angle Performance

The time constant obtained in the foregoing section is valid when the system operates within its linear dynamic range. Typically, the vehicle control system will be designed such that the relation $\ell_1 > \ell_3 > \ell_2$ holds among the limits of Fig. 2. ℓ_3 is the limit of despin motor capacity and the former inequality insures that all available motor torque may be used as required for maintaining platform despin whereas the latter insures that the despin loop will have dominant control. We assume that this relation holds and address nutation damping behavior when ℓ_2 is saturated and ℓ_1, ℓ_3 remain unsaturated. A more general case is perhaps best addressed by simulation. Denoting the maximum linear range for nutation damping as θ_m, we get

$$\theta_m = \ell_2/[Kr_0\sigma(2-\sigma)\omega_s^2] \tag{29}$$

by equating ℓ_2 to the peak torque from Eqs. (14) and (15). For angles θ_n larger than θ_m, ℓ_2 will saturate and the feedback gain K_n can be replaced by an equivalent describing function K_n^*. For a symmetric hard limit, the describing function approaches the limiting value

$$K_n^* \rightarrow K_n 4\ell_2/\pi T_n \tag{30}$$

where T_n is the input sinusoidal torque command. Substituting for K_n and T_n

$$K_n^* \rightarrow (4\ell_2/\pi)(\rho_0/\sigma^2\omega_s^2\theta_n) \tag{31}$$

We have noted previously the inverse proportionality of damping time constant τ_d with K_n, so Eq. (31) indicates an approximately linear increase in damping time constant with nutation after saturation of limit ℓ_2. This rather mild degradation is a desirable feature of this active damper mechanization.

V. Design Example

To illustrate the application of this nutation controller and to verify the predicted performance characteristics, an example design was performed for a spacecraft modeled after the INTELSAT IVA synchronous orbit communication satellite (shown in Fig. 1). The mass properties and parameters of the model assumed in the design are given in Table 1. The pointing control system for the design illustration utilizes the rotor-mounted pulse-data error sampling system of the form described in Sec. II.

To insure attitude stability, a stabilzing time constant below 100 sec over the entire range of nutation frequencies must be provided once the spacecraft is on-station. Simple active nutation control using the platform control system is limited

Table 1 Design example: system parameters and performance characteristics

Parameter/Characteristic	Symbol	Value
Rotor spin rate (design range)	ω_s	45–75 rpm (55 rpm nominal)
Transverse inertia over mission	I_T	1385 to 940 slug-ft^2
Despun payload inertia	I_p	154 slug-ft^2
Despun payload product of inertia	I_{23}	11.4 slug-ft^2
Vehicle inertia ratio over mission	σ	0.22 to 0.28
Accelerometer radius	r_0	3.25 ft
Accelerometer filters	$F_1(s)$	$(5.7\times10^4 s)/[(s+0.48)(s+20)(s+25)(s+110)]$
	$N_C[\lambda]$	$3.24s/[(s+0.75)(s+2.5)]$
Despin loop transmission	$H(s)$	$\frac{7.3\times10^5}{I_p(\omega_s-\omega_p)}\left[\frac{1-e^{-sT}}{s}\right]\left[\frac{(s+0.05)(s+0.63)}{s^3[s^2+2(0.5)(11)s+(11)^2]}\right]$
Nutation feedback gain (nominal)	K_n	6.9 ft-lb/ft/sec^2 (6.25 ft-lb/deg @55 rpm)
Net phase angle (nominal)	ϕ	$-156°$
Pointing disturbance	θ_p/θ_n	1.2:1
Dynamic range		0.5° of nutation
Nominal damping time constant ($\omega_p = 0$)	τ_d	75 sec (one motor on)
		38 sec (both motors on)

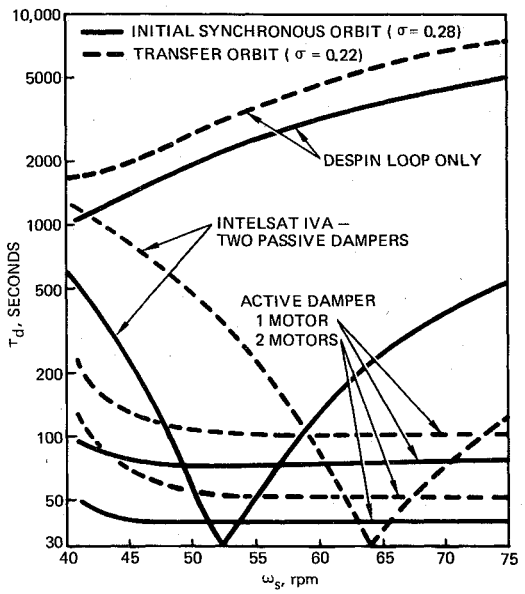

Fig. 7 Nutation damping time constant as a function of spin speed ($\omega_p = 0$).

severely by the moderate platform *POI* of 11.4 slug-ft^2. Without nutation feedback, the minimum achievable time constant will be ~1100 sec with an "optimum" control system design. Thus, to provide the active control required to stabilize this spacecraft, a tenfold increase in damping effectiveness is required.

The nutation controller design parameters and operating characteristics selected for this illustration are summarized in Table 1. The accelerometer pre- and postmodulation filters were selected to provide minimum gain and phase variations over the design range of nutation frequency. The total phase angle ϕ ($-156°$ for this design, based on the pointing control system dynamics shown) is set by physical alignment of the *SAE* output phase with the accelerometer. The linear range of $\pm 0.5°$ of nutation far exceeds the expected 0.05° level of nutation induced during attitude and orbit correction maneuvers. The transient azimuth pointing disturbances of 1.2 times the nutation angle provides an acceptable error during the worst-case nutation transient.

Performance of the active nutation controller is summarized in Fig. 7, which graphs the nutation damping time constant as a function of rotor spin rate for the two extremes of vehicle inertia ratio. Included in the figure for comparison are similar performance characteristics for two passive dampers designed for INTELSAT IVA, and the active damping achievable without nutation feedback. For initial synchronous orbit operation, the example design provides a broadband time constant of 75 sec for all spin rates above 50 rpm, with a factor of two improvement achievable (to 38 sec) if both of the redundant torque motors are activated.

The implication of the required tuning of the mechanical passive dampers is seen in both the degradation in damping time constant as the spin speed deviates from resonance and also in the shift in resonant spin rate as the vehicle inertia ratio changes between transfer and synchronous orbit. The passive damper effectiveness can vary by as much as 2000% if no steps are taken to maintain system operation near their resonance.

Verification of the analysis and evaluation of the control concept was carried out in a detailed analog computer simulation. Results from the simulation studies are presented in Table 2 and Fig. 8. Shown in the table are comparisons of predicted and measured active damping time constants for various control system parameters and for spinning and despun payload conditions. Very good agreement was found between the analytical predictions based on the closed-form solution derived in Sec. IV, and the simulation measurements. Simulation time response data illustrating system operation for several of the conditions listed in Table 2 are given in Fig. 8. No passive damping or destabilizing effects are included in these simulation responses, illustrating only the effect of active nutation control using the torque motor. The initial residual damping shown in the figures prior to activation of the nutation feedback controller is due to the minimal (>1100 sec) time constant resulting from simple dynamic coupling. Figure 8a shows the system response with a net phase angle ϕ of $-180°$. The figure shows the time history of several system state variables during a 0.03° amplitude nutation transient. The difference in nutation frequency between the accelerometer output and the transverse rates in platform coordinates can be seen in the lower two traces of the figure. The transformed accelerometer output signal can be observed in the second trace, showing the spin axis motor torque. The azimuth pointing error developed during the transient is seen in the top trace showing the despun payload boresight deviation from a nominal direction.

VI. Concluding Remarks

This paper has presented a technique to provide substantial active nutation control for dual-spin spacecraft configurations. Use of the inherent coupling between the spin axis dynamics and vehicle nutation through the despun payload product of inertia, in conjunction with direct nutation sensing via a rotor-mounted accelerometer, is shown to provide active stabilization equivalent or superior to that achievable with passive damping mechanisms. Analysis of the total closed-

Table 2 Comparison of simulated and analytical time constants, $\omega_s = 55$ rpm

ω_p, rpm	θ, deg	β	K, lb-sec^2	ϕ, deg	τ_d, sec Eq. (21)	τ_d, sec Analog simulat.	Figure number
0	−146	0	6.9	−180	116	117	
↑	↑	0	13.8	↑	58	58	
↕	↕	0.48	6.9	↕	81	82	Fig. 8a
↕	↕	0.24	↕	↕	95	94	
↓	↓	0.80	↕	↓	98	100	
0	−146	0.95	↕	−180	151	147	
2	−146	0.6	↕	−186	67	68	Fig. 8b
3	−147	0.67	↕	−189	66	60	
5	−148	0.89	↕	−197	132	113	
6	−149	2.1	↕	−201	−101	−110	
−2	−147	0.39	↕	−175	106	104	
−3	−147	0.36	↕	−173	124	125	Fig. 8c
0	−146	0.48	↕	−156	74	75[a]	Fig. 8d
0	−146	0.95	6.9	−156	85	90	

[a] Baseline design.

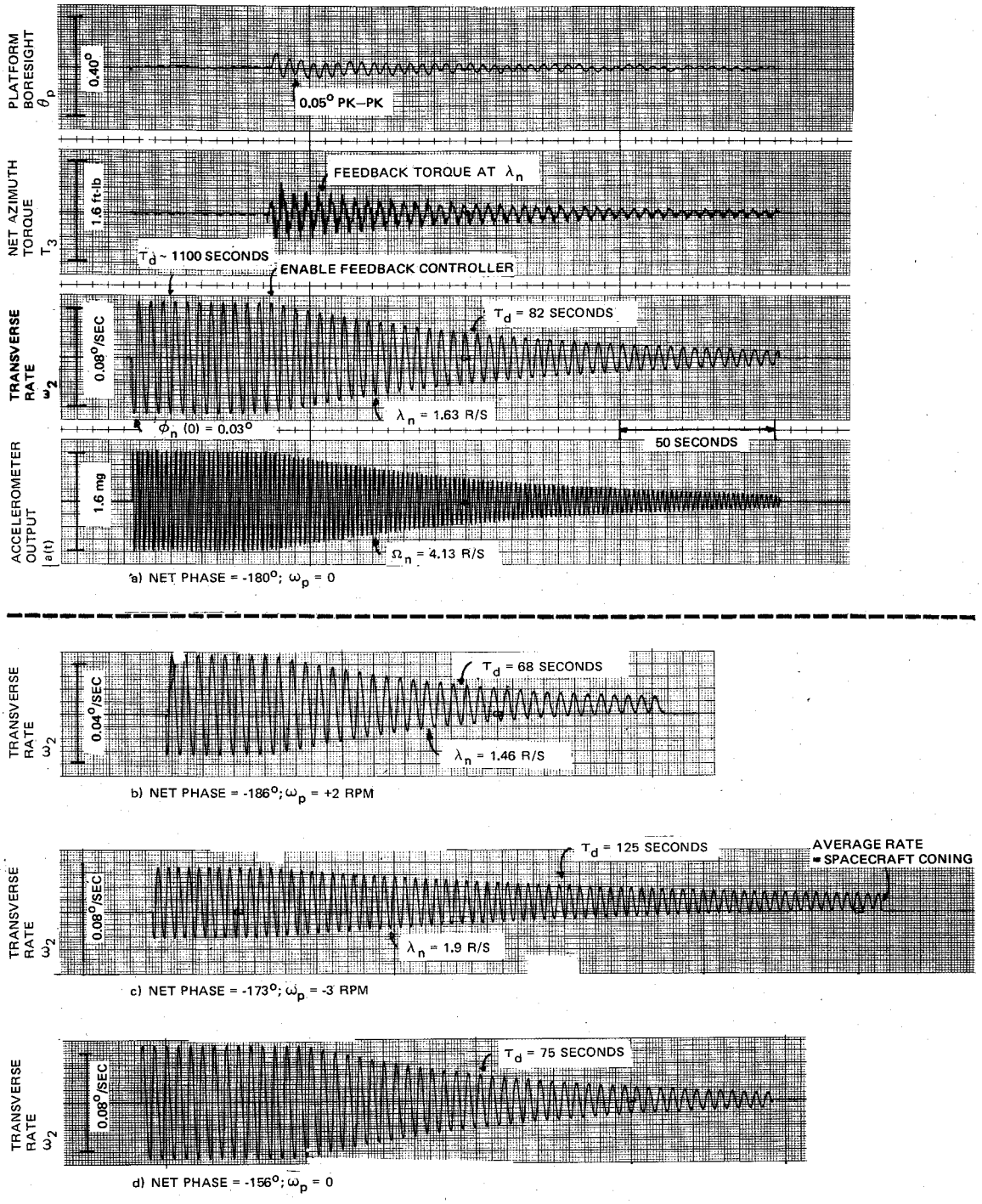

Fig. 8 Simulation time response during nutation transient.

loop system dynamics provided design and analysis tools which can be used to achieve an optimum dynamic response and also for easy evaluation of performance sensitivity to system parameters and vehicle mass properties. Electronic breadboarding and simulation studies have verified both the predicted performance of the technique and the ease in integration of the nutation controller into an existing control system design. This technique has been developed as an experiment on the COMSTAR I synchronous orbit domestic communication satellite built for COMSAT General Corportation and AT&T by Hughes Aircraft Company. Flight data from the first two COMSAT I spacecraft has shown the technique to be an extremely effective method of achieving nutation control, with measured in-orbit performance in excellent agreement with analytical predictions.

References

[1] Iorillo, A.J., "Analysis Related to the Hughes Gyrostat System," Highes Aircraft Co., Los Angeles, Calif., Rept. SSDT0438B, Dec. 1967.

[2] Likins, P.W., "Attitude Stability Criteria for a Dual-Spin Spacecraft," *Journal of Spacecraft and Rockets,* Vol. 4, April 1967, pp. 1638–1643.

[3] Mingori, D.L., "Effects of Energy Dissipation on the Attitude Stability of Dual Spin Satellites," *AIAA Journal,* Vol. 7, Jan. 1969, pp. 20–27.

[4] Neer, J.T., "Intelsat IV Nutation Dynamics," AIAA 4th Communications Satellite Conference, AIAA Paper 72-537, 1972, Washington, D.C.

[5] Phillips, K.J., "Active Nutation Damping Utilizing Spacecraft Mass Properties," *IEEE Transactions on Aerospace and Electronic Systems,* Vol. AES-9, Sept. 1973.

[6]Phillips, K.J., "Linearization of the Closed-Loop Dynamics of a Dual Spin Spacecraft," *Journal of Spacecraft and Rockets,* Vol. 8, Sept. 1971, pp. 938–945.

[7]Leliakov, I.P. and Barba, P.M., "Damping Spacecraft Nutation by Means of a Despun Antenna," *AAS/AIAA Astrodynamics Conference,* Vail, Colo., 1973.

[8]Slafer, L.I. and Marbach, H.D., "Active Control of the Dynamics of a Dual-Spin Spacecraft," *Journal of Spacecraft and Rockets,* Vol. 12, May 1975, pp. 287–293.

[9]Grasshoff, L.H., "An Onboard, Closed-Loop, Nutation Control System for a Spin Stabilized Spacecraft," *Journal of Spacecraft and Rockets,* Vol. 5, May 1968, pp. 530–535.

[10]Horowitz, I.M., *Synthesis of Feedback Systems,* Academic Press, New York, 1963, pp. 236.